

Enhancing urban real-time PM_{2.5} monitoring in street canyons by machine learning and computer vision technology



Zhiguang Fan^a, Yuan Zhao^{a,*}, Baicheng Hu^a, Li Wang^b, Yuxuan Guo^a, Zhiyuan Tang^a, Junwen Tang^a, Jianmin Ma^c, Hong Gao^a, Tao Huang^a, Xiaoxuan Mao^a

^a Key Laboratory for Environmental Pollution Prediction and Control, Gansu Province, College of Earth and Environmental Sciences, Lanzhou University, Lanzhou 730000, China

^b Collaborative Innovation Center for Western Ecological Safety, Lanzhou University, Lanzhou 730000, China

^c Laboratory for Earth Surface Processes, College of Urban and Environmental Sciences, Peking University, Beijing 100871, China

ARTICLE INFO

Keywords:

PM_{2.5}
Urban roads
Street view
Traffic image
Computer vision technology
Extreme gradient boosting

ABSTRACT

During peak hours, both pedestrians and drivers face extended exposure to road air pollution, raising the risk of respiratory diseases. Variations in traffic volume, building attributes, and weather conditions in street canyons lead to differing exposure levels across road sections and intersections. Though deploying numerous sensors provides real-time access to PM_{2.5} levels in each road section, they cannot interpret the impact of weather, traffic, and buildings on these levels. Therefore, in Lanzhou City, we attempted to use Computer Vision Technology (CVT) to extract real-time traffic volume and street-view features from traffic images for PM_{2.5} concentration prediction, and to interpret the impact of road environment changes on PM_{2.5} levels. Results show that by using the Extreme Gradient Boosting (XGB) regression model, the coefficient of determination for PM_{2.5} prediction reaches R²=0.956. Meteorological conditions, traffic volume, and buildings are key variables in predicting road PM_{2.5} concentrations. Meteorological conditions control the continuous fluctuation of road PM_{2.5} levels, while traffic volume can lead to sudden changes in PM_{2.5} levels. The research indicates that the combination of traffic cameras and CVT can acquire road PM_{2.5} concentrations, contributing significantly to rapidly understanding road pollution status, identifying highly polluted roads, and conducting exposure assessments of roadways.

1. Introduction

Urbanization has led to a substantial increase in the urban population and human health exposure risk in China (Fan et al., 2022; Hu & Zhao, 2022; Singh et al., 2021; Zhu et al., 2021). The heavy traffic in cities is considered as the main source of fine particulate matter (PM_{2.5}) (Askariyah et al., 2020; Li & Managi, 2021; Luo & Liao, 2015; Sánchez-Ccoyllo et al., 2009). Therefore, gaining a comprehensive understanding of air pollution characteristics in proximity to roadways can provide a basis for identifying the sources of roadway pollution and evaluating associated exposure risks. The increase in particulate matter on the road may be caused by fuel combustion, vehicle component wear, and dust resuspension. PM_{2.5} is a complex mixture of inorganic and organic constituents that cause adverse health outcomes (Guidoni et al., 2020; Peng et al., 2021; Yang et al., 2020). PM_{2.5} exposure has been linked to respiratory diseases in epidemiological studies and aerosol transmission of coronavirus in recent years (Tang et al., 2020; Wang

et al., 2021). The high density of vehicles and pedestrian flow during peak commuting hours may augment the health risks for commuters. However, sparse fixed-site monitoring is inadequate, adding further difficulties to understanding the real-time evolution of PM_{2.5} pollution on city roads (Buonanno et al., 2011; Steffens et al., 2012).

Extensive studies were conducted to assess on-road air pollution and its exposure risks to commuters. These studies utilize portable mobile monitoring devices for mobile tracking or fixed-point monitoring, capturing the spatiotemporal variations of particle concentration at high temporal and spatial resolutions. They take into account various factors during commuting in urban road microenvironments, such as meteorological conditions, commuting types, and traffic volume (Kumar et al., 2018; Qiu et al., 2017; Targino et al., 2016). Furthermore, certain studies extend their focus beyond mere monitoring, taking into account urban environmental factors. By optimizing the multi-dimensional spatial morphology of urban street canyons and increasing the coverage of urban green spaces, these studies identify potential avenues

* Corresponding author.

E-mail address: zhaoyuan@lzu.edu.cn (Y. Zhao).

for alleviating urban air pollution (O'Regan et al., 2022; Wang et al., 2022). Typically, these studies comprehensively integrate field observations, computational fluid dynamics models, physical simulations, and empirical models to develop a holistic understanding of road air pollution and exposure risks faced by commuters in different scenarios and locations (Fu et al., 2017; Zhang et al., 2015). Traffic volume and vehicle type are crucial in determining primary PM_{2.5} and precursor emissions (Li et al., 2022; Xu et al., 2022), but real-time monitoring of these factors on a city scale is challenging. Despite the existence of established methods, as noted by Khan et al. (2018), "Using traditional techniques of RADAR, LIDAR, and LASAR to address this problem is time-consuming, expensive, and tedious." Overall, existing methods for studying road air pollution have their respective limitations. The coverage of field observations is constrained by deployment and maintenance costs. Computational Fluid Dynamics (CFD) models demand substantial resources and may yield uncertain results. Physical simulations are confined by experimental conditions. Empirical models are constrained by data acquisition and may perform inadequately when handling new scenarios. Hence, considering the high cost and computations involved, these traditional approaches are often not implemented on larger spatial and temporal scales in cities.

To obtain the spatial segmentation characteristics of air pollutants in urban areas, land use models and mobile monitoring have been employed extensively (Apte et al., 2017; Patton et al., 2015; Zwack et al., 2011). Mobile monitoring requires recurring air pollutant sampling along a street, accompanied by simultaneous measurements of meteorological conditions (Hankey et al., 2019). Novel methods were developed by combining empirical models, mobile monitoring, and computer vision technology (CVT) to achieve more accurate and higher spatially resolved urban air pollution forecasting. In these methods, detailed street canyon features, such as roads, buildings, vegetation, and vehicles, were extracted from Google Street View through the CVT (O'Regan et al., 2022). These features were implemented in the quantitative assessment of fine and ultrafine particles, such as black carbon, PM₁, and PM_{2.5} in city streets (Liu et al., 2021; Lloyd et al., 2021; Lu et al., 2021; Qi & Hankey, 2021). While these methods pave new ways for air pollution predictions on a street scale, the street canyon features are not captured in real time by Google Street View or Baidu Street View (Kerckhoff et al., 2022; Meng et al., 2020; Yu et al., 2022). Although roads, buildings, and evergreen vegetation are seldom altered, vehicles, as major emission sources, on the road vary substantially. In some studies, street mobile monitoring was conducted, and the results were compared with street view images to establish the relationships between real-time traffic and street images, thereby improving the short-term spatial distribution of air pollutants on urban roads (Messier et al., 2018). The advantage of mobile air quality monitoring lies in its ability to increase the spatial resolution of measurements to the sub-street level, but at the cost of temporal sparsity at any given location. However, mobile monitoring does not facilitate for continuous temporal observations at fixed locations, thus limiting the ability to discern fine-grained temporal variations in particulate matter, despite capturing spatial changes effectively. Moreover, constrained by costs, fixed monitoring stations face difficulties in achieving the same spatial coverage as mobile monitoring. As a result, striking a balance between capturing temporal details of road pollution and expanding coverage to additional locations of interest poses a significant challenge.

To overcome these challenges, our aim is to develop an urban road air pollution assessment model that leverages the extensive deployment of traffic cameras at intersections. This model will utilize real-time traffic imagery to obtain live road PM_{2.5} concentrations, thereby acquiring real-time pollution information for a greater number of city intersections. China has set up more than 1,500 air-quality monitoring stations. Each major city across the country has several to dozens of monitoring stations (Rohde & Muller, 2015). However, it's nearly impossible to individually cover every intersection to provide real-time atmospheric pollution concentrations. On the other hand, traffic

cameras have already covered nearly all major intersections in the city. If the direct retrieval of PM_{2.5} concentrations from traffic imagery becomes feasible, it would imply that the costs associated with deploying air quality sensors and atmospheric pollution monitoring equipment at intersections could be avoided. Simultaneously, this approach would also address the deficiency in spatial coverage density of monitoring stations. Along this line of thought, we conducted a field campaign to extract a fixed road environment and time-varying traffic characteristics from road images integrated with semantic segmentation and object detection technology. The extracted data were combined with PM_{2.5} concentrations sampled via portable monitoring instruments and meteorological instruments to train and establish the road PM_{2.5} forecasting models subject to well-established image recognition techniques. The aim was to obtain better PM_{2.5} forecasting results compared to the previously reported empirical models. We have selected three PM_{2.5} sampling points for model training and analysis, and an additional twenty sites to evaluate the extrapolation capability of the model. The objective of the present study was to explore real-time PM_{2.5} assessment approaches by using traffic camera images of roads and intersections and to facilitate data acquisition under different real-life street air pollution scenarios.

2. Materials and methods

2.1. Sampling sites

Lanzhou City in northwestern China is featured by a mountain-valley topography and has a population of ~4.38 million. The Congestion Delay Index (CDI) can reflect the traffic congestion situation of a city, where a CDI ≥ 1.5 indicates congestion. Among the 77 cities in China, Lanzhou's highest CDI reaches 2.75, ranking 14th in terms of average CDI, and the CDI during specific hours indicates that congestion mainly occurs during the commuting peak (Wei et al., 2022). We selected Chengguan District as the target area of Lanzhou for model development because this district accounts for 34 % of the city's population and is the most densely populated area with traffic congestion. Considering the variations in traffic congestion during weekdays and weekends, we ensured that our sampling covered a span of one week. We collected road data for three sites over the course of a week, aiming to establish and test the method's predictive capability with a minimal number of samples. This approach will provide crucial insights into the sampling strategy and associated costs. It's important to note that a richer sample set typically enhances method performance, incorporating a diverse range of weather conditions, seasons, road situations, and urban characteristics over the long term and across a wide area. Moreover, the intra-week variations in road pollution are not to be ignored. Our current focus is on testing the feasibility of the method at a low cost. Therefore, we selected a week from the same season for the sampling period, aligning with our objectives of cost-effectiveness. As shown in Fig. 1, we selected three road intersections for collecting street view images, meteorological data, and PM_{2.5} concentration. These three sites have different characteristics in terms of road environment and traffic flow, and are located in areas with different types of land use (Fig. S1). The data collected at Sites 1–3 were used for training the models at these sites, PM_{2.5} and meteorological variables were sampled continuously for 1 week during the traffic rush hour in the morning (8:00–9:00) and evening (17:00–18:00) daily. As traffic control (COVID-19 prevention and control measures) was conducted at Site 1 from March 31 to April 6, 2022, to compare the difference in traffic between the rush hour and normal time, another 7-day sampling was conducted at Site 1 during this period. Although these three training sites can be utilized for model development and evaluating the PM_{2.5} concentration prediction capability at the sampling sites, it is not possible to ascertain whether the model is capable of predicting other sites within the city. In other words, verifying the model's extrapolation capability requires additional intersection samples for validation. The additional twenty sites, referred

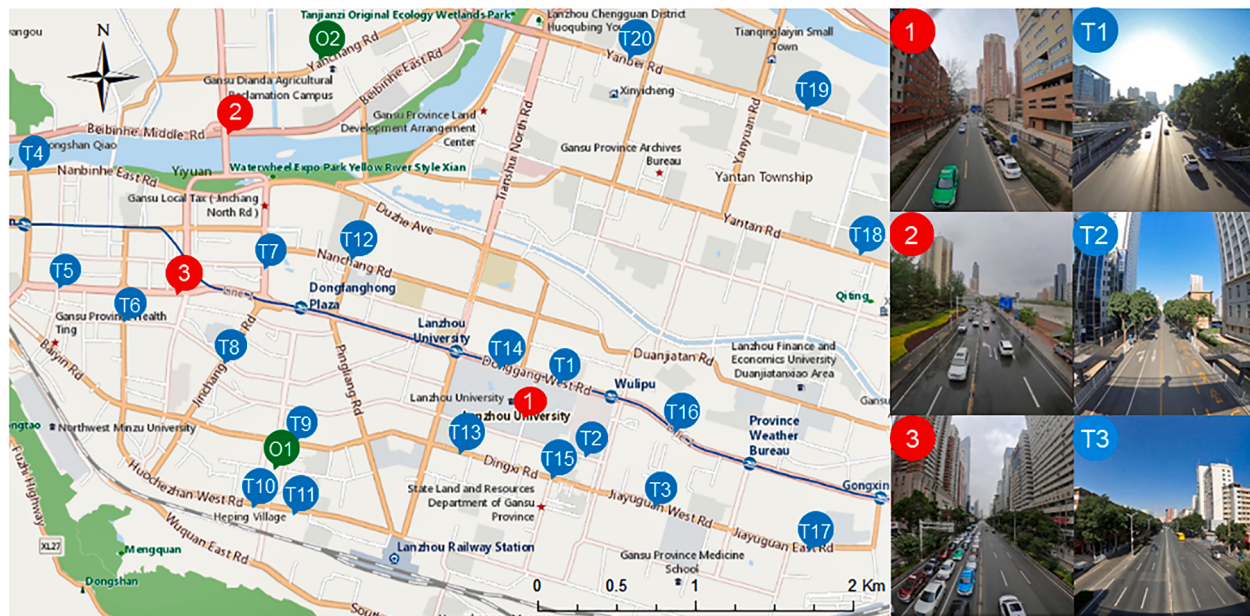


Fig. 1. Locations of the three training sites 1 to 3 (red), the twenty evaluation sites T1 to T20 (blue), and the two official air quality monitoring stations O1 and O2 (green).

to as T1 to T20, were sampled using the same method and solely used for evaluating the extrapolation capability of the model. Thus, we examined the extent to which the model based on road images from limited road intersections can be used in PM_{2.5} prediction for any other road and intersections without sampling data. The field sampling was conducted by the authors. Table S1 and Fig. S2 present the detailed sampling time and brief descriptions of road conditions for each site.

Based on the road characteristics in Lanzhou City, we had completed data collection by selecting three main road types with different underlying characteristics. Site 1 is adjacent to a university campus and witnesses a large number of pedestrians, particularly during and after dinner time. Site 2 is located on the Yellow River Bridge with multiple traffic lanes and is characterized by traffic congestion and vegetation

coverage. Sites 3 is located on the main road across the downtown of Lanzhou City and are characterized by dense traffic volume and pedestrians.

2.2. Street view process

2.2.1. Street view collection

We set up a camera on a traffic overpass so that the acquired traffic images provide an overview of the entire intersection. A panoramic camera (Max, GoPro, the USA) was used to record video data of traffic and road scenes. The video data were extracted in a 2 s interval to match the frequency of meteorology data and PM_{2.5} sampling. Each frame of the extracted video data was used for counting vehicles and for license

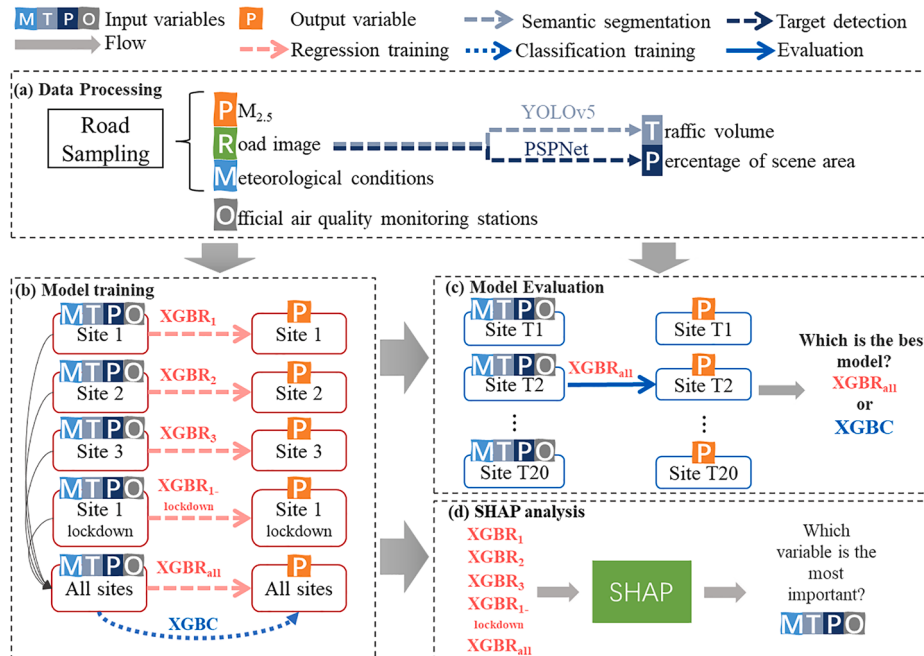


Fig. 2. Flowchart of (a) data processing, (b) model training, (c) model evaluation, and (d) SHapley Additive exPlanation (SHAP) analysis.

plate recognition through a target detection technology (Fig. 2a).

2.2.2. Vehicle detection and license plate monitoring

To monitor the license plates of vehicles, we used a vision model termed “You Only Look Once (YOLOv5)”, a real-time object detection model (<https://github.com/ultralytics/yolov5>). This study focuses solely on the changes in PM_{2.5} concentration caused by vehicles traveling on the road, considering that such changes may arise from emissions generated by moving vehicles and resulting resuspension. The study excludes the impact of parked vehicles on PM_{2.5} (Fig. S3). Subsequently, the blue (gasoline-powered vehicles), green (new energy vehicles), and yellow (trucks and buses) license plates are separately used as input variables for statistical analysis. The average precision (AP) of YOLO v5 on the license plate data we collected is 85.5 % for blue, 84.3 % for green, and 76.5 % for yellow. More detailed information on the relationship between license plate color, vehicle type, and fuel type can be found in Text S1.

2.2.3. Road-scene parsing

To collect scene information, we used the semantic segmentation method called pyramid scene parsing network (PSPNet) (Sun & Zheng, 2022; Yang & Guo, 2022; Yuan et al., 2022; Yue et al., 2022), which is a scene parsing model that provides the proportion of different moving and fixed objects on each road scene in the whole picture of a street (<https://github.com/bubbliiing/pspnet-pytorch>), more details in Text S2. Based on the actual road scenes in the current study, we configured seven categories within PSPNet, including buildings, mountains, the sky, vegetation, roads, rivers, and others. In the current study, these categories already encompass the vast majority of elements present in street scenes. Except for the “Others” category, the PSPNet model achieved the highest mean Intersection over Union (mIoU) of 83.6 % among the 6 object categories. Although some objects, such as mountain areas and river areas, had relatively low Intersection over Union (IoU) values of around 39 %, the majority of detected objects had IoU values exceeding 70 %, such as road areas (93.8 %), sky areas (97.7 %), vegetation areas (94.5 %), and building areas (73.0 %). Each scene type was calculated as a percentage of the image area, and these percentages were used as input variables for PM_{2.5} evaluation models.

2.3. Meteorological data

We collected meteorological data at the all sites. The data included temperature, relative humidity, atmospheric pressure, and wind speed using a portable weather station (Kestrel 5500, Nielsen-Kellerman, USA) with a sampling frequency of 2 s. Wind speed data was collected only for wind parallel to the road. These meteorological variables were used to examine the response of the PM_{2.5} sampled at road intersections to real-time meteorological conditions because these conditions often determine the formation and dispersion of PM_{2.5}.

2.4. PM_{2.5} at intersections

PM_{2.5} concentrations at the all sites were measured by DustTrak™ II Aerosol Monitor 8532 (TSI-8532 DUSTTRAK, the USA) with a sampling frequency of 2 s. TSI-8532 is a portable instrument with an accuracy of $\pm 0.001 \text{ mg/m}^3$ and a range of 0.001–150 mg/m³. Additional sampling device information can be found in Table S2. Before sampling, we compared the sampling results of TSI-8532 with those of the Lanzhou Atmospheric Components Monitoring Superstation to ensure that TSI-8532 obtains a consistent time series of PM_{2.5} concentration features with the fixed monitoring station (Fig. S4). The Pearson correlation coefficient between the two was 0.877. Zero calibration was performed before each sampling, and data exceeding the measurement range of the device were excluded after sampling. We also used hourly PM_{2.5} concentration data collected from official air quality monitoring stations as an input feature for our model, this concentration can be considered as

the background concentration. The official hourly PM_{2.5} concentrations collected from the nearest official air-quality monitoring station are available on the website of the China National Environmental Monitoring Center (<http://air.cnemc.cn/>). Fig. 1 shows the location of the all sites and two official air-quality monitoring stations (O1 and O2).

2.5. Modeled PM_{2.5} evaluation

Research has already demonstrated that the real-time variation of PM_{2.5} concentration at traffic intersections is influenced by meteorological conditions, traffic patterns, and the built environment of the intersections (Xu et al., 2022). Based on the aforementioned assumptions, extreme gradient boosting (XGB) is currently chosen as the evaluation model. XGB model utilizes gradient boosting algorithm and regularization techniques to adapt to complex nonlinear relationships, effectively control model complexity, mitigate overfitting risks, and enhance accuracy. The detailed of XGB can be found in (Chen & Guestrin, 2016). Additionally, XGB demonstrates fast execution speed and interpretability, providing insights into prediction results through feature importance computation. We established extreme gradient boosting regression (XGBR) models and collected street view, meteorological, and PM_{2.5} official air-quality monitoring data to train our road intersection PM_{2.5} forecasting model. As shown in Fig. 2b, to include the impact of meteorological conditions and road scenes in the model, we built five XGBR regression models (Fig. 2c). The first model integrates all the data at Sites 1–3 to train the XGBR_{all} model, and the remaining four models were built using data at Sites 1–3 and Site 1 again for the traffic control period, and these models are termed XGBR₁, XGBR₂, XGBR₃, and XGBR_{1-lockdown}, respectively. SHapley Additive exPlanation (SHAP) analysis was then performed in these five model simulations to quantify the contribution of each input variable to road PM_{2.5} (Fig. 2d). Notably, the road-scene features were only changed in XGBR_{all} among the five models. Therefore, we only focused on the effect of road scene on road PM_{2.5} in the SHAP analysis of XGBR_{all}. To determine the optimal sampling frequency, we compared the XGBR results obtained at sampling frequencies of 2, 4, 6, 8, and 10 s. More detailed parameters of the five XGBR models are provided in Table S3.

Models with extrapolation capabilities require less data, thereby reducing the costs associated with data collection and model training. We validated the extrapolation capabilities of the XGBR model by using twenty sites (T1-T20) that were not included in the training process. We compared its extrapolation performance with that of the an extreme gradient boosting for classification (XGBC) model. The XGBC adopted the same training data as XGBR_{all}, with the output data for PM_{2.5} concentration interval classification. To facilitate health assessment, PM_{2.5} concentrations were classified into six groups according to the World Health Organization guidelines (WHO Global Air Quality Guidelines, 2023). The range of each concentration classification is given in Table S4. Moreover, we considered the statistical distribution of the sampled data subject to the six concentration classifications to ensure that model performance was not affected by classification imbalance. The statistical probability density and data volume of each group of PM_{2.5} data were illustrated in Figs. S5 and S6.

We used a 10-fold cross-validation method with a total sample size of 92468, using 80 % shuffled data for the training model and the other data for estimating and testing model accuracy. The XGBR and XGBC models were built using the scikit-learn Python package, and the SHAP analysis of variable attributions was analyzed using the SHAP Python package, more method details are available in Text S3. We used XGBR and XGBC to predict the PM_{2.5} concentrations at Sites T1 to T20. The results were compared with the measured data to evaluate the extrapolation capability of the model (Fig. 2c). If a model trained on sites 1 to 3 can predict PM_{2.5} concentrations for sites T1 to T20, it has the potential to significantly reduce the cost of road PM_{2.5} monitoring.

3. Results

3.1. Road features and traffic

Based on the scene parsing of PSPNet, we obtained the percentage of underlying surface coverage in targeted streets, including buildings, mountains, the sky, vegetation, roads, rivers, and others. Fig. 3 displays the training sites 1 to 3 and the testing sites T1 to T3, while the remaining testing sites T4 to T20 are shown in Fig. S7. The scene analysis results indicate that, among all street scenes, roads are the most prominent feature. Furthermore, due to buildings obstructing the sky, there exists an inverse relationship between the proportions of buildings and the sky in the scene. Similarly, vegetation also exhibits a similar relationship in terms of obstructing buildings. The percentage of buildings and trees in the sky cover over targeting streets provides information about street width and building height on both roadsides. The height-to-width ratio (H/W) of a street is often used to estimate street canyon air pollution. In Fig. 3, the category “Others” represents scene elements that were not specifically classified but include road signs, sidewalks, and pedestrian guardrails. As shown in Fig. 3, Site 2 has a more open view than Sites 1 and 3, which are featured by taller buildings on roadsides. Site 3 is on a six-lane street with more vehicles on the road than Site 1, which is on a dual-lane street. As hills and rivers account for a very small portion of the road landscape, they were ignored in the road scenes.

The traffic volume data and license plate information related to Sites 1–3 during the 7-day measurement campaign were obtained by YOLOv5. Fig. S8 shows the total number of vehicles at Sites 1–3 in the morning and afternoon. Compact gasoline cars with blue license plates accounted for the highest number among all vehicles at all sites, followed by new energy vehicles with green plates, including hybrid electric vehicles and pure electric vehicles. Trucks and buses fueled by gasoline with a yellow license plate accounted for the lowest vehicle number. Most traffic congestion was observed at Site 3 as the main street and road traffic artery of the city, and the least traffic was observed at Site 1.

3.2. Road PM_{2.5} and meteorological conditions

We compared the sampled ambient PM_{2.5} at the sites with the

measured values at official air-quality monitoring stations nearest to these sites. The results are shown in Figs. S9 and S10. The road PM_{2.5} concentrations were considerably higher during the rush-hour traffic period, and the road median PM_{2.5} concentration was 1.58–2.07 times higher than the official measured data, particularly at Sites 2 and 3 on the main streets. High-concentration outliers were observed mainly at Sites 1 and 3. We conducted a further comparative analysis of the relationship between traffic volume and PM_{2.5} concentration. As depicted in Fig. S8d, the median PM_{2.5} concentration at Site 3 surpasses that of the fixed monitoring sites by 30 µg/m³. This difference stands as the highest among the three sites examined. Notably, Site 3 also holds the distinction of having the highest traffic volume among all sites. The Pearson correlation coefficient between the difference in PM_{2.5} median values from the sampling and fixed stations at the three sites and the total traffic volume is 0.972, indicating a positive correlation between them.

The air temperature measured every 2 seconds by the portable weather station was generally higher in the afternoon compared to the morning (see Fig. S11). The wind speeds were mostly less than or equal to 2 m/s (Fig. S12). The relative humidity tended to be stable with minimal fluctuations (Fig. S13).

3.3. Assessing modeled PM_{2.5} concentrations

3.3.1. XGBR performance and SHAP analysis

The XGBR models were trained to predict real-time PM_{2.5} concentrations at Sites 1–3 using collected road scenes, traffic volume, meteorological conditions, and background PM_{2.5} concentration. Here, for the training and performance evaluation of each model at Sites 1–3, the sampling data at the same sites were used. The coefficient of determination (R^2) among the five XGBR modules reached 0.956 (Figs. S14a and S15). The agreements between the predicted and sampled PM_{2.5} concentrations were also good in the high and low concentration ranges, as demonstrated using our randomly selected 500 test samples (Fig. S16).

The Shapley analysis of these five models for five group results revealed that PM_{2.5} background concentrations (collected from the official air-quality monitoring stations) and meteorological conditions are significant factors contributing to road PM_{2.5}, followed by road scenes and traffic volume. Fig. 4(a) illustrates the contributions of

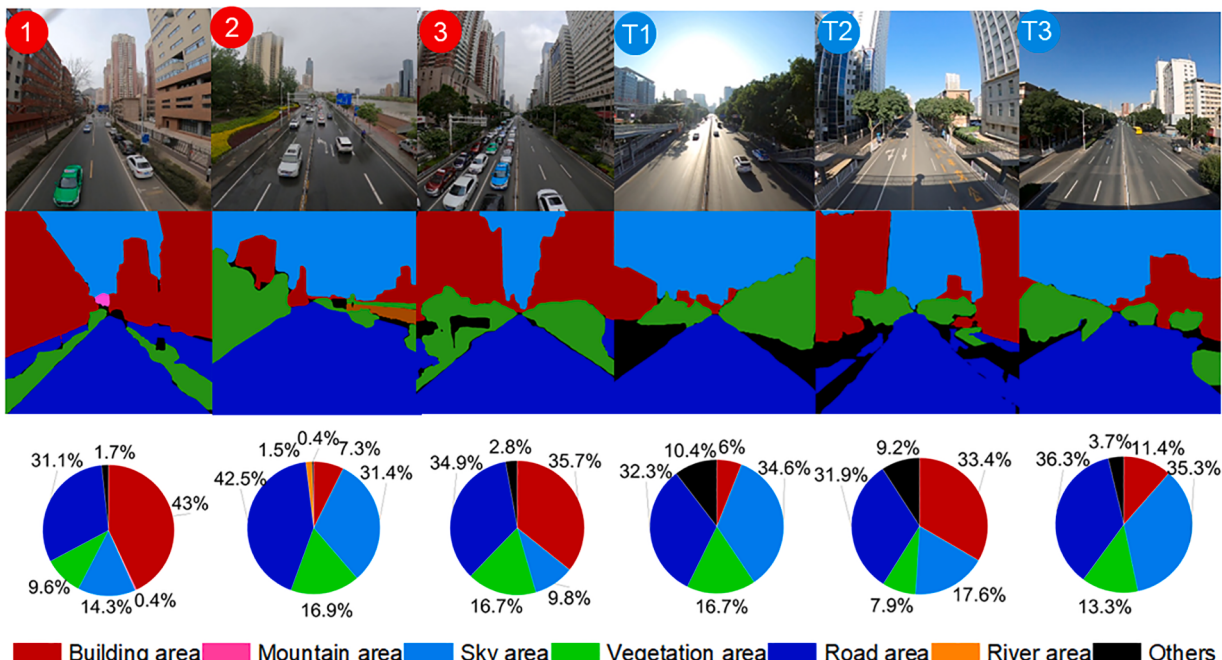


Fig. 3. Segments of seven categories of scenes and the percentage of area under each category.

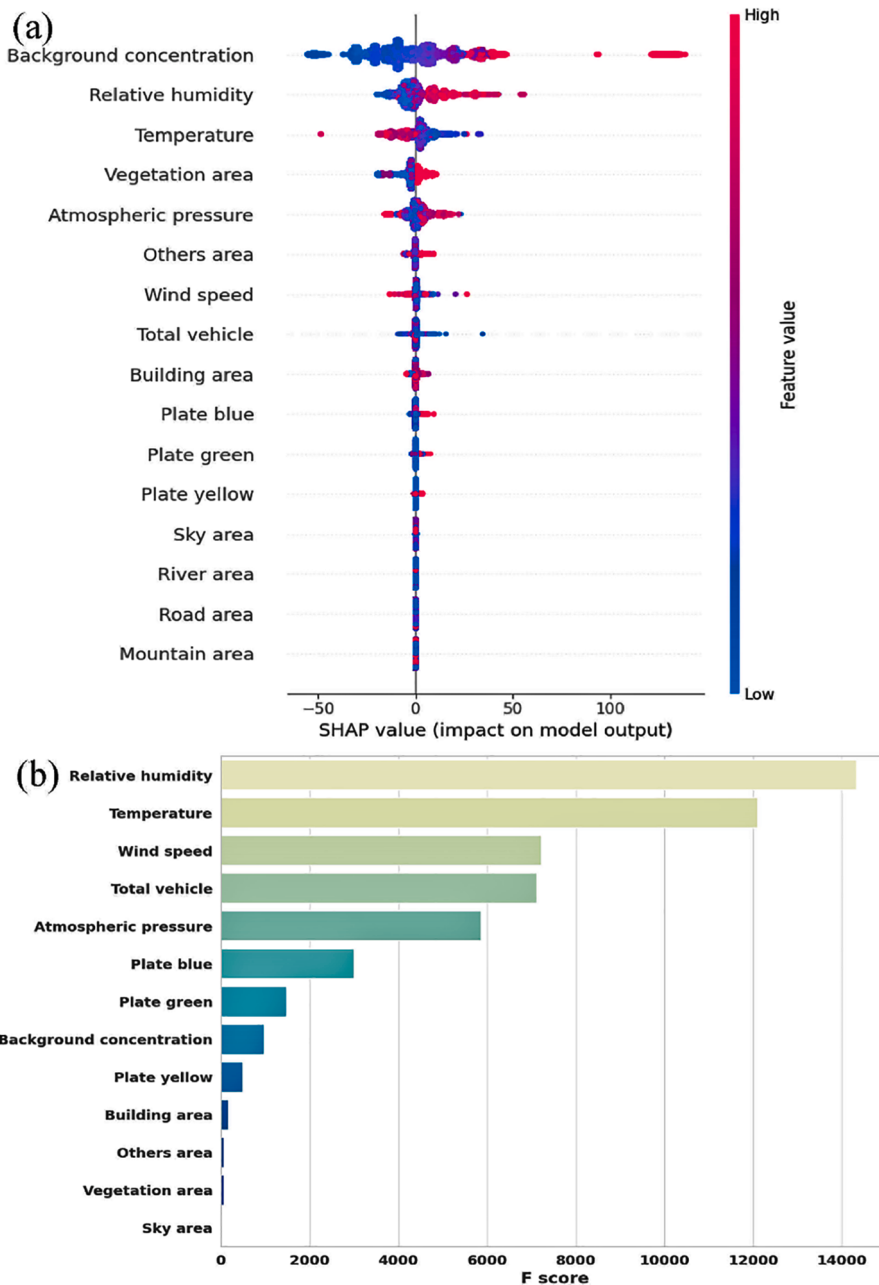


Fig. 4. Input variables based on SHAP values (a) and XGB feature score (b) are sorted in the XGBR_{all} model from top to bottom based on their significance.

different input variables of XGBR_{all} to the predicted PM_{2.5} concentrations, as determined by the Shapley analysis, ranked from high to low. At Sites 1–3, the highest SHAP values for background PM_{2.5} concentrations were positively correlated with real-time road PM_{2.5} concentrations. Among these meteorology variables, relative humidity and atmospheric pressure had a positive contribution to the modeled PM_{2.5}, whereas temperature had a negative contribution. The SHAP value of wind speed was zero, indicating that the wind speed did not make any significant contribution to the real-time road PM_{2.5} concentrations. For road scenes, the proportion of building-covered areas in the image was negatively correlated with the real-time road PM_{2.5} concentrations. Fig. S17 shows that among the input variables of XGBR₁, XGBR_{1-lockdown}, and XGBR₂ at Sites 1 and 2, the background PM_{2.5} concentration, meteorology, and traffic volume, in that order, were more important input variables. For Site 3, however, the input variables in the order of decreasing significance were meteorological factors, background PM_{2.5} concentration, and traffic volume.

The XGB feature importance analysis yielded feature scores (F score), where a higher feature score indicates a more important feature. Fig. 4 (b) presents the analysis results for XGBR_{all}, showing the features in descending order of importance: meteorological factors, traffic volume, background PM_{2.5} concentration, and road scenes. The importance of traffic volume is considered to be even more significant compared to the results obtained from the SHAP analysis. In both analyses, the building is the most important input variable in the road scene. SHAP analysis considers the interactions and dependencies among features, and its results are based on the range of values in the data. On the other hand, XGB feature importance tends to measure the direct contribution of features in the model, and its results are based on the model parameters. Despite the differences in methodology, interpretability, applicability, and robustness between SHAP analysis and XGB feature importance, we believe that both provide valuable insights into the importance of input features and should not be disregarded.

The model indicates that meteorological factors are significant

variables influencing the output of the model. We further compared the sampling data with fixed station data (Fig. S18) to validate the reasonableness of the meteorological data. We calculated correlation coefficients, yielding results of 0.689 for wind speed, 0.989 for temperature, 0.992 for relative humidity, and 0.996 for atmospheric pressure. It should be noted that the fixed monitoring stations were positioned on building rooftops, and wind speed data collected on the road was restricted to the direction parallel to the road, which might have contributed to the lower correlation of wind speed. Additionally, considering the seasonal variability of meteorological factors, the sampling data used for model training were limited to the spring season.

Considering that the model predicts the variation in PM_{2.5} concentration over a 2-second time interval, it is reasonable to suggest that the two most important features, meteorological factors and traffic volume, play a crucial role in inducing short-term changes in PM_{2.5} concentration. Additionally, when considering the respective predictive capabilities of these two feature categories for PM_{2.5} concentration (Fig. S19), meteorological factors exhibit a better predictive performance ($R^2=0.963$) compared to traffic volume ($R^2=0.063$). This implies that meteorological factors are likely associated with the continuous fluctuation of road PM_{2.5} concentration, while traffic volume may contribute to rapid, sporadic changes in PM_{2.5} concentration.

3.3.2. Model extrapolation capability evaluation

XGBR_{all} was constructed using data from sites 1-3 and exhibited good predictive performance ($R^2 = 0.956$) at these sites. However, its regression prediction capabilities were insufficient at the twenty additional sites from T1 to T20 (Table S6), indicating that XGBR_{all} lacks extrapolation ability. Therefore, we shifted our focus to evaluating the extrapolation capability of the XGBC model. The results in Fig. 5 indicate that XGBC performs significantly better than XGBR_{all}. Among the 20 testing sites, 60 % of the stations have an accuracy rate higher than 0.6. Additionally, there are 7 stations with accuracy rates exceeding 0.9. There are an additional 6 sites with accuracy below 0.2, and the remaining 7 sites have accuracy ranging from 0.4 to 0.9. Among them, site T1 achieved the highest accuracy of 0.998, while site T4 had a zero accuracy, indicating the lowest performance. The average accuracy of the 20 sites is 0.592.

4. Discussions

In the present study, efforts were made to assess the relation between road PM_{2.5} concentration and street view, meteorological conditions, and traffic volume using CVT. We aimed to further explore the potential applications of this approach to predict road PM_{2.5} concentrations. Our

results show that meteorological conditions, traffic volume, and street canyon morphology are the major factors contributing to the model predictability of road PM_{2.5} concentrations.

Roads and buildings are the predominant morphology of urban street canyons, which are closely related to the dispersion of atmospheric pollutants on roads. For example, the buildings at Sites 1 and 3 are taller than those at Site 2; the presence of buildings affects the sky cover, i.e., a low sky cover implies the presence of more buildings. The importance of the area under building cover and sky cover in predicting street PM_{2.5} concentrations can be discerned from the SHAP analysis. Mobile observations and computational fluid dynamics simulations of PM_{2.5} in street canyons often adopt a street aspect ratio (H/W) to estimate the removal of air pollutants. The street morphology of dense buildings can explain 37 % of the spatial variability of PM_{2.5} (He et al., 2017; Hu et al., 2021). Although the present study did not use H/W in the model, it is evident that Sites 1 and 3 have a greater H/W than Site 2 and are morphologically symmetrical, possibly causing more vortex formation—a condition that is not conducive to PM_{2.5} removal. This may be one of the reasons for the higher PM_{2.5} concentrations at Sites 1 and 3 compared to Site 2 (Yazid et al., 2014).

High relative humidity and pressure showed a positive correlation with PM_{2.5}; however, temperature did not show any clear relationship with PM_{2.5}. Previous studies showed that high relative humidity is not conducive to the dispersion of pollutants but favors the formation of secondary PM_{2.5} on streets (Huang et al., 2016). The frequent occurrence of stable stratification and calm wind conditions because of the valley–mountain topography in Lanzhou City do not favor the dispersion of air pollutants but rather cause the accumulation of pollutants (Deaves & Lines, 1998). The effect of temperature on the dispersion of pollutants in street canyons, on the one hand, can be attributed to thermal instability, which helps to carry air pollutants out of the atmospheric boundary layer. On the other hand, street morphology and wind direction can cause the opposite effect on pollutant removal, causing pollutants to accumulate near the ground surface on the roadside of the street. As shown in Fig. S17, atmospheric pressure has a significant positive correlation with PM_{2.5} concentrations at Site 3. At Site 1, the positive correlation between atmospheric pressure and PM_{2.5} is weaker but still clear. In contrast, at Site 2, this relationship is not clear. Based on the current analytical methods, it is difficult for us to delve deeper into the differences in variable contributions among different sites in the black box model. However, the global variable importance given by the current methods has already demonstrated the significance of meteorological factors.

Vehicles are the main source of mobile emissions on roads. The combined effect of wind speed, wind direction, street canyon

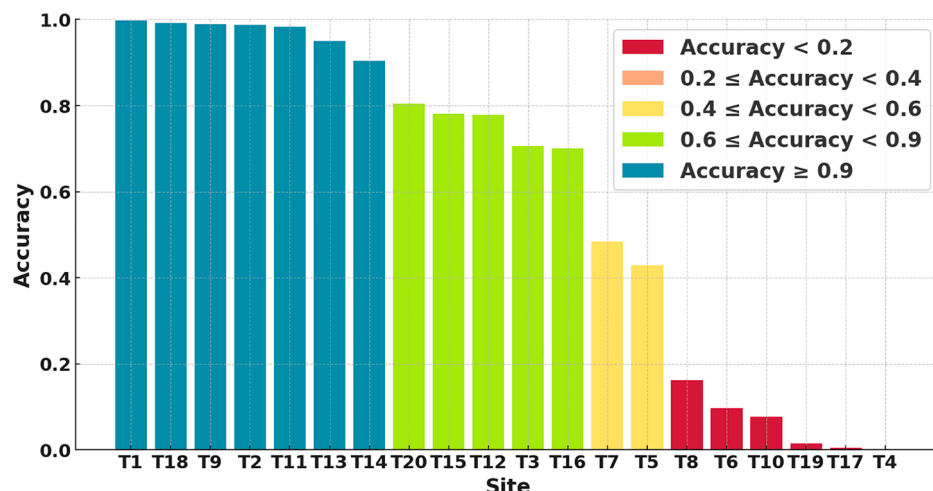


Fig. 5. The XGBC model evaluates the accuracy of sites T1 to T20 (Red bars: <0.2, orange bars: 0.4~0.9, and yellow bars: >0.9).

morphology, vehicle speed, and vehicle travel direction may increase the spread of air pollutants on the road and also enhance the removal of PM_{2.5} from street canyons. In our study, Site 3, which had the highest traffic volume, tended to have a higher PM_{2.5} level; however, Sites 1 and 2 did not show any clear relationship with PM_{2.5}. Fuel vehicles with blue license plates exerted a greater impact on road PM_{2.5} concentrations than the other vehicle types. However, our research cannot differentiate whether the contribution of vehicles to road PM_{2.5} originated from dust kicked up by the moving vehicles or vehicle emissions.

The model's objective is to predict the PM_{2.5} concentration, and there is indeed a disparity in the predictive performance of the XGBR model across different sites. Fig. S15b distinctly points out that the model performance at Site 1 is inferior to others, while both Fig. S15 and Fig. S16 demonstrate that there are more high values of PM_{2.5} at Site 1. We compared the statistical distributions of predicted and sampled concentrations, as illustrated in Fig. S20a. The model exhibits a significant error in predicting high PM_{2.5} concentrations, whereas the distribution of predicted values aligns with the distribution of sampled values for concentrations below 220 µg/m³ (Fig. S20b). Therefore, the deficiency in predicting high values is likely a crucial factor contributing to the decline in model performance and the ensuing uncertainty in the model outcomes. It is worth noting that the XGB method is an ensemble model approach, having amalgamated the distributions of multiple output results. Therefore, defects of predicting high concentrations is more likely to be attributed to the scarcity of data in high-concentration scenarios.

The outcomes of the model's input-output variables have provided insights into the distinct roles played by meteorological conditions, nearby road-adjacent building morphology, and traffic emissions in influencing road PM_{2.5} concentrations. Segments with towering buildings on either side of the road, high traffic flow, and urban areas characterized by unfavorable dispersion-conducive meteorological conditions warrant particular attention in assessing PM_{2.5} exposure during commuting. It is imperative to implement both fixed and mobile monitoring in these segments routinely to ascertain potential long-term exposure among commuting individuals during peak hours.

Currently, the utilization of road imagery data for PM_{2.5} exposure assessment demonstrates the respective advantages of regression and classification models. Regression models offer more precise predictive outcomes, while classification models possess latent transferability potential. However, it is essential to consider that limitations persist in the current model framework. Firstly, meteorological data, a pivotal variable influencing PM_{2.5} concentration disparities at different road intersections, still necessitate additional equipment for acquisition. Secondly, real-world traffic imagery may differ from our collected data in aspects such as resolution, color, and scene coverage, potentially impacting the model's results. Moreover, despite the transferability showcased by classification models, their stability remains insufficient for practical application, thereby requiring further development and validation within authentic scenarios.

In conclusion, our findings affirm the applicability of utilizing traffic imagery to predict real-time variations in road PM_{2.5} concentrations and for exposure assessment. Furthermore, this method facilitates the analysis of the effects of variables such as meteorology, building attributes, and traffic flow on PM_{2.5} concentrations at different road intersections. The potential for transferability also positions this method to potentially capture urban road atmospheric pollution characteristics at a higher spatiotemporal resolution.

5. Conclusions

In this study, we attempted to establish a model framework to predict road PM_{2.5} pollution using street view images captured by traffic cameras in a city and a machine-learning model. We show that the machine-learning model provides excellent performance in road PM_{2.5} prediction. The model achieves good accuracy in road PM_{2.5} forecasting with a

relatively small sample size. Street view provides additional information on vehicles and road environments, making it an important variable for PM_{2.5} prediction on roads. However, when it comes to rapid fluctuations in PM_{2.5} concentration on the road, meteorological conditions play a more significant role.

The extrapolation capability of a model is crucial in determining the cost reduction potential in practical applications. The current method has shown outstanding extrapolation capability at some sites, indicating its potential for application. However, considering the current instability of extrapolation results, the application of the current research findings in real road scenarios still appears insufficient. Nevertheless, with improvements in the model framework and data, this low-cost method for predicting road PM_{2.5} has the potential to become a reality. We look forward to similar methods being tested in more cities. With the help of artificial intelligence techniques, we anticipate that utilizing existing public infrastructure, such as traffic cameras, can provide urban environmental and public health managers with richer tools and information.

Supporting Information

Sampling sites information; Sampling instruments; Parameters and performance of models; Classification and statistics distribution of PM_{2.5} concentration; SHAP value; Comparison results of PM_{2.5} concentrations at road sampling and regular air quality monitoring stations; Comparison results of meteorological parameters and hourly data from nearby fixed stations; Introduction to PSPNet and SHAP Methods.

Declaration of Competing Interest

The authors declare that they have no known competing financial interests or personal relationships that could have appeared to influence the work reported in this paper.

Data availability

Data will be made available on request.

Acknowledgments

The work was supported by the National Natural Science Foundation of China (42107106), the Youth Science and Technology Fund Project of Gansu Province of China (grants 21JR7RA524 and 21JR7RA528). Supported by Supercomputing Center of Lanzhou University.

Supplementary materials

Supplementary material associated with this article can be found, in the online version, at [doi:10.1016/j.scs.2023.105009](https://doi.org/10.1016/j.scs.2023.105009).

References

- Apte, J. S., Messier, K. P., Gani, S., Brauer, M., Kirchstetter, T. W., Lunden, M. M., Marshall, J. D., Portier, C. J., Vermeulen, R. C. H., & Hamburg, S. P. (2017). High-resolution air pollution mapping with google street view cars: Exploiting big data. *Environmental Science & Technology*, 51, 6999–7008. <https://doi.org/10.1021/acs.est.7b00891>
- Askariyah, M. H., Venugopal, M., Khreis, H., Birt, A., & Zietsman, J. (2020). Near-road traffic-related air pollution: Resuspended PM_{2.5} from highways and arterials. *IJERPH*, 17, 2851. <https://doi.org/10.3390/ijerph17082851>
- Buonanno, G., Fuoco, F. C., & Stabile, L. (2011). Influential parameters on particle exposure of pedestrians in urban microenvironments. *Atmospheric Environment*, 45, 1434–1443. <https://doi.org/10.1016/j.atmosenv.2010.12.015>
- Chen, T., & Guestrin, C. (2016). XGBoost: A scalable tree boosting system. In *Proceedings of the 22nd ACM SIGKDD International Conference on Knowledge Discovery and Data Mining* (pp. 785–794). <https://doi.org/10.1145/2939672.2939785>
- Deaves, D. M., & Lines, I. G. (1998). The nature and frequency of low wind speed conditions. *Journal of Wind Engineering and Industrial Aerodynamics*, 73, 1–29. [https://doi.org/10.1016/S0167-6105\(97\)00278-X](https://doi.org/10.1016/S0167-6105(97)00278-X)

- Fan, W., Xu, L., & Zheng, H. (2022). Using multisource data to assess PM_{2.5} exposure and spatial analysis of lung cancer in Guangzhou, China. *LJERPH*, 19, 2629. <https://doi.org/10.3390/ijerph19052629>
- Fu, X., Liu, J., Ban-Weiss, G. A., Zhang, J., Huang, X., Ouyang, B., Popoola, O., & Tao, S. (2017). Effects of canyon geometry on the distribution of traffic-related air pollution in a large urban area: Implications of a multi-canyon air pollution dispersion model. *Atmospheric Environment*, 165, 111–121. <https://doi.org/10.1016/j.atmosenv.2017.06.031>
- Guidoni, D. L., Maia, G., Souza, F. S. H., Villas, L. A., & Loureiro, A. A. F. (2020). Vehicular traffic management based on traffic engineering for vehicular ad hoc networks. *IEEE Access*, 8, 45167–45183. <https://doi.org/10.1109/ACCESS.2020.2978700>
- Hankey, S., Sforza, P., & Pierson, M. (2019). Using mobile monitoring to develop hourly empirical models of particulate air pollution in a rural appalachian community. *Environmental Science & Technology*, 53, 4305–4315. <https://doi.org/10.1021/acs.est.8b05249>
- He, L., Hang, J., Wang, X., Lin, B., Li, X., & Lan, G. (2017). Numerical investigations of flow and passive pollutant exposure in high-rise deep street canyons with various street aspect ratios and viaduct settings. *Science of The Total Environment*, 584–585, 189–206. <https://doi.org/10.1016/j.scitotenv.2017.01.138>
- Hu, H., Chen, Q., Qian, Q., Lin, C., Chen, Y., & Tian, W. (2020). Impacts of traffic and street characteristics on the exposure of cycling commuters to PM_{2.5} and PM10 in urban street environments. *Building and Environment*, 188, Article 107476. <https://doi.org/10.1016/j.buildenv.2020.107476>
- Hu, Y., & Zhao, B. (2022). Indoor sources strongly contribute to exposure of Chinese urban residents to PM_{2.5} and NO₂. *Journal of Hazardous Materials*, 426, Article 127829. <https://doi.org/10.1016/j.jhazmat.2021.127829>
- Huang, X., Liu, Z., Zhang, J., Wen, T., Ji, D., & Wang, Y. (2016). Seasonal variation and secondary formation of size-segregated aerosol water-soluble inorganic ions during pollution episodes in Beijing. *Atmospheric Research*, 168, 70–79. <https://doi.org/10.1016/j.atmosres.2015.08.021>
- Kerckhoffs, J., Khan, J., Hoek, G., Yuan, Z., Hertel, O., Ketzel, M., Jensen, S. S., Al Hasan, F., Meliefste, K., & Vermeulen, R. (2022). Hyperlocal variation of nitrogen dioxide, black carbon, and ultrafine particles measured with Google street view cars in Amsterdam and Copenhagen. *Environment International*, 170, Article 107575. <https://doi.org/10.1016/j.envint.2022.107575>
- Khan, S., Ali, H., Ullah, Z., & Bulbul, M. F. (2018). An intelligent monitoring system of vehicles on highway traffic. In *2018 12th International Conference on Open Source Systems and Technologies (ICOSSST)* (pp. 71–75). <https://doi.org/10.1109/ICOSSST.2018.8632192>
- Kumar, P., Patton, A. P., Durant, J. L., & Frey, H. C. (2018). A review of factors impacting exposure to PM_{2.5}, ultrafine particles and black carbon in Asian transport microenvironments. *Atmospheric Environment*, 187, 301–316. <https://doi.org/10.1016/j.atmosenv.2018.05.046>
- Li, C., & Managi, S. (2021). Contribution of on-road transportation to PM_{2.5}. *Sci Rep*, 11, 21320. <https://doi.org/10.1038/s41598-021-00862-x>
- Li, Q., Liang, S., Xu, Y., Liu, L., & Zhou, S. (2022). Assessing personal travel exposure to on-road PM_{2.5} using cellphone positioning data and mobile sensors. *Health & Place*, 75, Article 102803. <https://doi.org/10.1016/j.healthplace.2022.102803>
- Liu, X., Zhang, X., Schnelle-Kreis, J., Jakobi, G., Cao, X., Cyrys, J., Yang, L., Schlotter-Hai, B., Abbaszade, G., Orasche, J., Khedr, M., Kowalski, M., Hank, M., & Zimmermann, R. (2021). Spatiotemporal characteristics and driving factors of black carbon in Augsburg, Germany: combination of mobile monitoring and street view images. *Environmental Science & Technology*, 55, 160–168. <https://doi.org/10.1021/acs.est.0c04776>
- Lloyd, M., Carter, E., Diaz, F. G., Magara-Gomez, K. T., Hong, K. Y., Baumgartner, J., Herrera, G. V. M., & Weichenthal, S. (2021). Predicting Within-City spatial variations in outdoor ultrafine particle and black carbon concentrations in Bucaramanga, Colombia: A hybrid approach using open-source geographic data and digital images. *Environmental Science & Technology*, 55, 12483–12492. <https://doi.org/10.1021/acs.est.1c01412>
- Lu, T., Marshall, J. D., Zhang, W., Hystad, P., Kim, S.-Y., Bechle, M. J., Demuzere, M., & Hankey, S. (2021). National empirical models of air pollution using microscale measures of the urban environment. *Environmental Science & Technology*, 55, 15519–15530. <https://doi.org/10.1021/acs.est.1c04047>
- Luo, H., & Liao, L. (2015). The study on the emission list of fine particulate matter, which are discharged from the traffic flow source in Guilin. In *Proceedings of the 2015 International Conference on Economics, Social Science, Arts, Education and Management Engineering Presented at the 2015 International Conference on Economics, Social Science, Arts, Education and Management Engineering*. Xi'an, China: Atlantis Press. <https://doi.org/10.2991/essame-15.2015.156>
- Meng, L., Wen, K.-H., Zeng, Z., Brewin, R., Fan, X., & Wu, Q. (2020). The impact of street space perception factors on elderly health in high-density cities in Macau—analysis based on street view images and deep learning technology. *Sustainability*, 12, 1799. <https://doi.org/10.3390/su12051799>
- Messier, K. P., Chambliss, S. E., Gani, S., Alvarez, R., Brauer, M., Choi, J. J., Hamburg, S. P., Kerckhoffs, J., LaFranchi, B., Lunden, M. M., Marshall, J. D., Portier, C. J., Roy, A., Szpiro, A. A., Vermeulen, R. C. H., & Apte, J. S. (2018). Mapping air pollution with Google street view cars: Efficient approaches with mobile monitoring and land use regression. *Environmental Science & Technology*, 52(21), 12563–12572. <https://doi.org/10.1021/acs.est.8b03395>
- O'Regan, A. C., Byrne, R., Hellebust, S., & Nyhan, M. M. (2022). Associations between Google street view-derived urban greenspace metrics and air pollution measured using a distributed sensor network. *Sustainable Cities and Society*, 87, Article 104221. <https://doi.org/10.1016/j.scs.2022.104221>
- Patton, A. P., Zamore, W., Naumova, E. N., Levy, J. I., Brugge, D., & Durant, J. L. (2015). Transferability and generalizability of regression models of ultrafine particles in urban neighborhoods in the Boston area. *Environmental Science & Technology*, 49, 6051–6060. <https://doi.org/10.1021/es5061676>
- Peng, L., Shen, Y., Gao, W., Zhou, J., Pan, L., Kan, H., & Cai, J. (2021). Personal exposure to PM_{2.5} in five commuting modes under hazy and non-hazy conditions. *Environmental Pollution*, 289, Article 117823. <https://doi.org/10.1016/j.envpol.2021.117823>
- Qi, M., & Hankey, S. (2021). Using street view imagery to predict street-level particulate air pollution. *Environmental Science & Technology*, 55, 2695–2704. <https://doi.org/10.1021/acs.est.0c05572>
- Qiu, Z., Xu, X., Song, J., Luo, Y., Zhao, R., Zhou, B. X. W., Li, X., & Hao, Y. (2017). Pedestrian exposure to traffic PM on different types of urban roads: A case study of Xi'an, China. *Sustainable Cities and Society*, 32, 475–485. <https://doi.org/10.1016/j.scs.2017.04.007>
- Rohde, R. A., & Muller, R. A. (2015). Air pollution in china: mapping of concentrations and sources. *PLoS ONE*, 10, Article e0135749. <https://doi.org/10.1371/journal.pone.0135749>
- Sánchez-Ccoyo, O. R., Ynoue, R. Y., Martins, L. D., Astolfo, R., Miranda, R. M., Freitas, E. D., Borges, A. S., Fornaro, A., Freitas, H., Moreira, A., & Andrade, M. F. (2009). Vehicular particulate matter emissions in road tunnels in São Paulo, Brazil. *Environ Monit Assess*, 149, 241–249. <https://doi.org/10.1007/s10661-008-0198-5>
- Singh, P., O'Toole, T. E., Conklin, D. J., Hill, B. G., & Haberzettl, P. (2021). Endothelial progenitor cells as critical mediators of environmental air pollution-induced cardiovascular toxicity. *American Journal of Physiology-Heart and Circulatory Physiology*, 320, H1440–H1455. <https://doi.org/10.1152/ajpheart.00804.2020>
- Steffens, J. T., Wang, Y. J., & Zhang, K. M. (2012). Exploration of effects of a vegetation barrier on particle size distributions in a near-road environment. *Atmospheric Environment*, 50, 120–128. <https://doi.org/10.1016/j.atmosenv.2011.12.051>
- Sun, Y., & Zheng, W. (2022). HRNet- and PSPNet-based multiband semantic segmentation of remote sensing images. *Neural Comput & Applic*. <https://doi.org/10.1007/s00521-022-07737-w>
- Tang, S., Mao, Y., Jones, R. M., Tan, Q., Ji, J. S., Li, N., Shen, J., Lv, Y., Pan, L., Ding, P., Wang, X., Wang, Y., MacIntyre, C. R., & Shi, X. (2020). Aerosol transmission of SARS-CoV-2: Evidence, prevention and control. *Environment International*, 144, Article 106039. <https://doi.org/10.1016/j.envint.2020.106039>
- Targino, A. C., Gibson, M. D., Krecl, P., Rodrigues, M. V. C., Dos Santos, M. M., & De Paula Correa, M. (2016). Hotspots of black carbon and PM_{2.5} in an urban area and relationships to traffic characteristics. *Environmental Pollution*, 218, 475–486. <https://doi.org/10.1016/j.envpol.2016.07.027>
- Wang, C. C., Prather, K. A., Sznitman, J., Jimenez, J. L., Lakdawala, S. S., Tufekci, Z., & Marr, L. C. (2021). Airborne transmission of respiratory viruses. *Science*, 373, eabd9149. <https://doi.org/10.1126/science.abd9149>
- Wang, W., Cheng, X., & Dai, M. (2022). Strategies for sustainable urban development and morphological optimization of street canyons: Measurement and simulation of PM_{2.5} at different points and heights. *Sustainable Cities and Society*, 87, Article 104191. <https://doi.org/10.1016/j.scs.2022.104191>
- Wei, X., Ren, Y., Shen, L., & Shu, T. (2022). Exploring the spatiotemporal pattern of traffic congestion performance of large cities in China: A real-time data based investigation. *Environmental Impact Assessment Review*, 95, Article 106808. <https://doi.org/10.1016/j.eiar.2022.106808>
- WHO Global Air Quality Guidelines: particulate matter (PM2.5 and PM10), ozone, nitrogen dioxide, sulfur dioxide and carbon monoxide [WWW Document], 2023. URL <https://www.who.int/publications-detail-redirect/9789240034228> (accessed 3.18.23).
- Xu, J., Zhang, M., Ganji, A., Mallinen, K., Wang, A., Lloyd, M., Venuta, A., Simon, L., Kang, J., Gong, J., Zamel, Y., Weichenthal, S., & Hatzopoulou, M. (2022). Prediction of short-term ultrafine particle exposures using real-time street-level images paired with air quality measurements. *Environmental Science & Technology*, 56, 12886–12897. <https://doi.org/10.1021/acs.est.2c03193>
- Yang, C., & Guo, H. (2022). A method of image semantic segmentation based on PSPNet. *Mathematical Problems in Engineering*, 2022, 1–9. <https://doi.org/10.1155/2022/8958154>
- Yang, J., Shi, B., Zheng, Y., Shi, Y., & Xia, G. (2020). Urban form and air pollution disperse: Key indexes and mitigation strategies. *Sustainable Cities and Society*, 57, Article 101955. <https://doi.org/10.1016/j.scs.2019.101955>
- Yazid, A. W. M., Sidik, N. A. C., Salim, S. M., & Saqr, K. M. (2014). A review on the flow structure and pollutant dispersion in urban street canyons for urban planning strategies. *Simulation*, 90, 892–916. <https://doi.org/10.1177/0037549714528046>
- Yu, X., Her, Y., Huo, W., Chen, G., & Qi, W. (2022). Spatio-temporal monitoring of urban street-side vegetation greenery using Baidu Street View images. *Urban Forestry & Urban Greening*, 73, Article 127617. <https://doi.org/10.1016/j.ufug.2022.127617>
- Yuan, W., Wang, J., & Xu, W. (2022). Shift pooling PSPNet: rethinking PSPNet for building extraction in remote sensing images from entire local feature pooling. *Remote Sensing*, 14, 4889. <https://doi.org/10.3390/rs14194889>
- Yue, H., Xie, H., Liu, L., & Chen, J. (2022). Detecting people on the street and the streetscape physical environment from baidu street view images and their effects on community-level street crime in a Chinese city. *IJGI*, 11, 151. <https://doi.org/10.3390/ijgi11030151>

Zhang, H., Xu, T., Zong, Y., Tang, H., Liu, X., & Wang, Y. (2015). Influence of meteorological conditions on pollutant dispersion in street canyon. *Procedia Engineering*, 121, 899–905. <https://doi.org/10.1016/j.proeng.2015.09.047>

Zhu, C., Maharajan, K., Liu, K., & Zhang, Y. (2021). Role of atmospheric particulate matter exposure in COVID-19 and other health risks in human: A review.

Environmental Research, 198, Article 111281. <https://doi.org/10.1016/j.envres.2021.111281>

Zwack, L. M., Paciorek, C. J., Spengler, J. D., & Levy, J. I. (2011). Modeling spatial patterns of traffic-related air pollutants in complex urban terrain. *Environmental Health Perspectives*, 119, 852–859. <https://doi.org/10.1289/ehp.1002519>